Journal of ELECTRONIC MATERIALS, Vol. 46, No. 1, 2017
DOI: 10.1007/s11664-016-4873-y

Influence of Annealing Temperature on CZTS Thin Film Surface Properties

WENMEI FENG,[1] JUNFENG HAN,[1,4,5,6] JUN GE,[1] XIANGLIN PENG,[1] YUNONG LIU,[1] YU JIAN,[1] LIN YUAN,[1] XIAOLU XIONG,[1] LIMEI CHA,[2] and CHENG LIAO[3]

1.—School of Physics, Beijing Institute of Technology, Beijing 100081, China. 2.—College of Materials Science and Engineering, Hunan University, Changsha 410082, China. 3.—College of Materials Science and Engineering, Beijing University of Technology, Beijing 100124, China. 4.—*Present address:* School of Physics, Beijing Institute of Technology, Beijing 100081, China. 5.—e-mail: pkuhjf@gmail.com. 6.—e-mail: pkuhjf@bit.edu.cn

In this work, copper zinc tin sulfide (CZTS) films were deposited by direct current sputtering and the samples were annealed in different oven-set temperatures and atmosphere (Ar and H_2S). The surface evolution was investigated carefully by using scanning electron microscopy (SEM), Raman spectroscopy and x-ray photoelectron spectroscopy. The surface of the as-sputtered precursor contained little Cu and large amounts of Zn and Sn. The metallic precursor was continuous and compact without pinholes or cracks. With the increase of the temperature from room temperature to 250°C, Cu atoms diffused to the film surface to form $Cu_{1-x}S$ and covered other compounds. Some small platelets were smaller than 500 nm spreading randomly in the holes of the film surfaces. When the temperature reached 350°C, Zn and Sn atoms began to diffuse to the surface and react with S or $Cu_{1-x}S$. At 400°C, SEM showed the melting of large particles and small particles with a size from 100 nm to 200 nm in the background of the film surface. Excess Zn segregated towards the surface regions and formed ZnS phase on the surface. In addition, the signal of sodium in the CZTS surface was observed above 400°C. At 600°C, a large amount of regular structures with clear edges and corners were observed in the film surface in SEM images. A clear recrystallized process on the surface was assumed from those observations.

Key words: CZTS thin films, surface, sputtering, raman, XPS

INTRODUCTION

Chalcopyrite semiconductors are promising materials for high-efficiency and low-cost thin film solar cells.[1,2] The most popular chalcopyrite photovoltaic material is copper indium gallium selenide (CIGS).[3] Interestingly, the laboratory CIGS solar cell efficiency has reached 21%.[4] However, indium and gallium are scarce elements in the earth and widely used in many different applications including microelectronics.[5] This has led to the limitation of mass production of CIGS modules in the mid- to long-term. Therefore, earth-abundant photovoltaic materials have become more and more popular in the last few years.[6–8] Among those materials, copper zinc tin sulfide (CZTS) has become one of the most popular and promising candidates.[9]

CZTS is a *p*-type semiconductor with kesterite crystal structure. The high absorption coefficient and the direct band gap of about 1.5 eV make it an ideal absorber material for photovoltaic applications.[10] Recently, different interesting CZTS thin film deposition routes have been developed, such as co-evaporation,[11] sulfite of metallic precursor,[12] nano-ink printing[13] and electrical deposition,[14] and efficiencies have reached 12.6%.[15] However, formation of secondary phases in the CZTS film is

(Received March 19, 2016; accepted August 11, 2016; published online August 30, 2016)

the major issue which limits CZTS solar cell device performance.[16,17] Due to the narrow phase formation region, the optimized composition ranges for high-performance devices are Cu/(Zn+Sn) between 0.80 and 0.95, and Zn/Sn between 1.05 and 1.25.[18,19] To improve CZTS solar cell device performance, many research groups are trying to understand and eliminate the secondary phase formation.[20,21] Chen et al.[22] has provided defect physics of the CZTS layer properties. The understanding of the surface evaluation properties of the CZTS layer during the sulfide process is also important but there are only a few publications available on this topic. As we know, the semiconductor film surface plays an important role as part of the hetero-junction of photovoltaic devices. Therefore, to gain more information on materials processing, it is necessary to investigate in detail the crystalline structure of the surface under various annealing temperatures.

In this paper, we present the influence of annealing processes on CZTS film properties in an Ar+H_2S atmosphere. The main motivation of this work is to investigate modifications of the CZTS surface during the annealing processes. The surface morphologies of CZTS film can be visualized by a scanning electron microscope (SEM). The structures and chemical compositions were characterized by Raman spectroscopy and x-ray photoelectron spectroscopy (XPS). In this work, the influence of different annealing temperatures on CZTS film surface morphological and chemical properties were analyzed in detail.

EXPERIMENTAL

Film Deposition

Thin films were deposited on Mo-coated soda-lime glass substrates. In the first step, the metallic precursor films were deposited by co-sputtering Cu, Zn and Sn targets at an Ar pressure of 0.7 Pa. The substrate was not heated during the deposition, i.e. the deposition temperature was close to room temperature. The precursor film thickness ($\sim$1 μm) was measured by using a depth profilometer. Several similar samples were produced to anneal at different temperatures. The precursor films were then annealed in a tubular furnace in Ar+H_2S (20% H_2S) atmosphere (40 sccm). The H_2S gas serves as a sulfur source to diffuse into the film. The furnace pressure was maintained at 10 Pa. Each sample was annealed at a defined oven-set temperature (250°C, 300°C, 350°C, 400°C, 500°C, and 600°C). The heating rate was 20°C/min from room temperature and the holding time was 30 min.

Characterization

A Zeiss Supra 55 SEM was used to characterize the microstructures and morphologies. The Raman spectra were recorded in back-scattering geometry at room temperature, using a Jobin–Yvon Labram HR800 spectrometer with 325-nm and 633-nm laser lines. The shift in Raman peak was identified by using the literature records.[23,24] The XPS studies were performed using a Kratos ultra spectrometer with a monochromatized Al anode x-ray source ($h\nu$ = 1486.6 eV) equipped with an ion sputter-gun. Sputtering was performed with 1 kV Ar ions for 30 s leading to a typical sputtering depth of 1 nm. As a result, the CZTS film surface was exposed and the possible contaminations such as C and O were partially removed.

RESULTS AND DISCUSSION

Evolution of CZTS Thin Film Surface Morphologies Under Various Temperatures

Figure 1 shows the typical SEM images of annealed samples at each studied temperature. The change in the surface morphology is clearly seen. The metallic precursor is continuous and compact without pinholes or cracks as shown in Fig. 1a. At 250°C, the low annealing temperature (Fig. 1b), the film surface forms a porous structure with lot of pinholes and cracks among the grain boundaries. Those particle structures have sizes in the range of 0.5–2 μm. Some small platelets are smaller than 500 nm and distributed randomly in the holes of the film surfaces. At 300°C (Fig. 1c), these porous structures start to merge together near to the film surface. With a further increase in annealing temperature up to 350°C, a clear crystal growth phenomenon is observed (Fig. 1d). The film surface consists of particles larger than 2 μm spreading randomly in the surface. At 400°C, these particles lose their clear edges and seem to re-melt. Along with the larger grains, the film also consists of small particles with a size in the range of 100–200 nm (Fig. 1e). At 500°C annealing temperature, these particles grow up to 500 nm as shown in Fig. 1f, and simultaneously the surface becomes more compact and smooth. Finally, at 600°C, a significant change in surface microstructure is observed (Fig. 1g), and a large amount of regular structures with clear edges and corners can be seen on the film surface. We can conclude that a recrystallization process takes place at this temperature and leads to the formation of a compact morphological structure.

Raman Spectroscopy Characterization Under Various Annealing Temperatures

Figure 2 presents Raman spectra of the films. The Ramen spectra detection depth depends on the laser penetration depth which is estimated to be 100 nm with the 633-nm laser and less than 100 nm with the ultra-laser (325 nm). Figure 2a shows the Raman spectra measurements made using the 633-nm laser source. Initially, there is no peak in the metallic precursor. After sulfurization at 250°C,

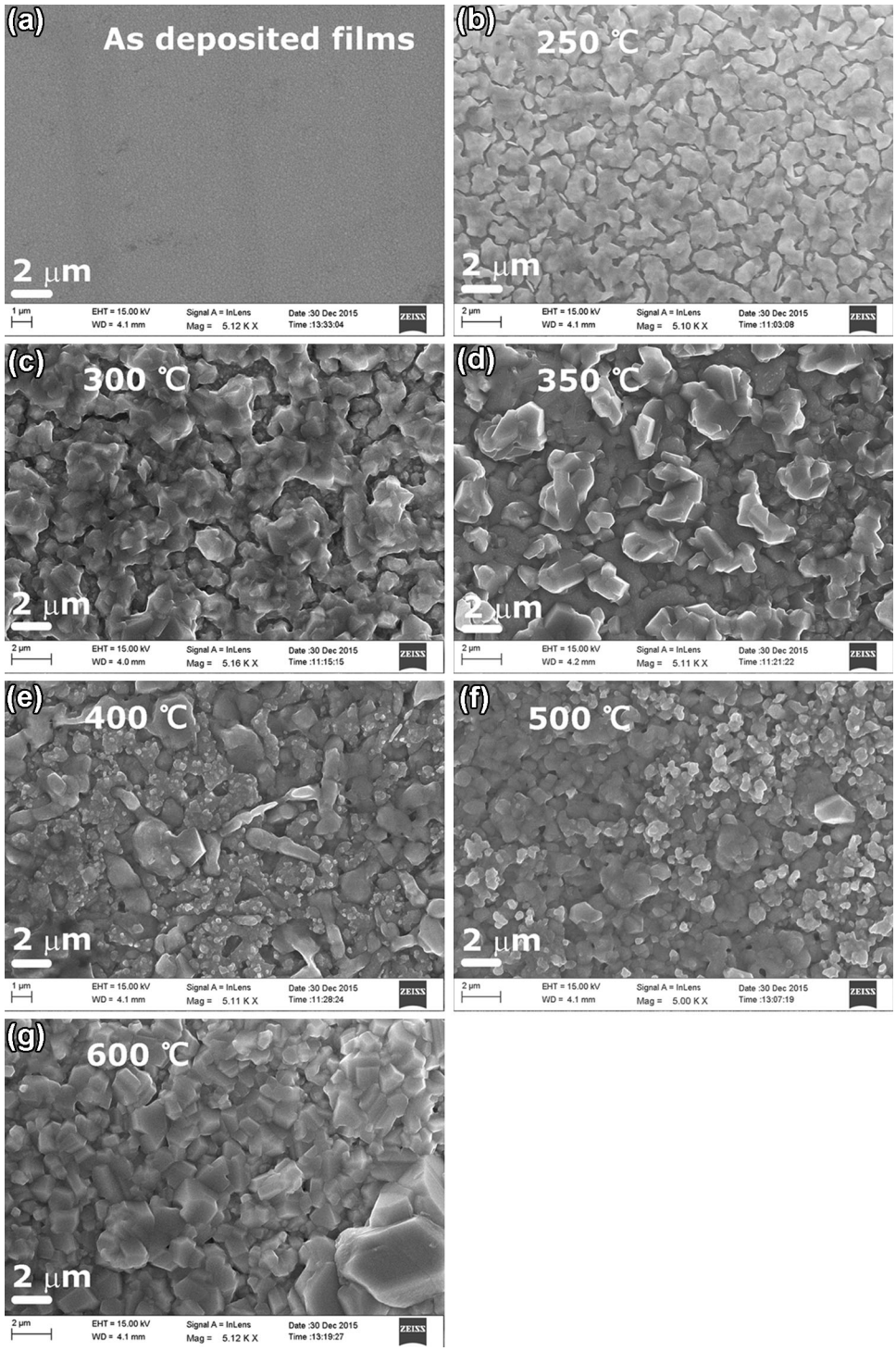

Fig. 1. SEM images of the as-deposited film and films annealed at various temperatures from 250°C to 600°C.

the film has an obvious peak at 475 cm^{-1} which belongs to $Cu_{2-x}S$. With the increase in annealing temperature (300°C and 350°C), the intensity of the peak increases. However, at higher annealing temperatures (>400°C), the peak intensity starts to decrease and then disappears. At 300°C, a rather weak peak at 352 cm^{-1} is observed and we believe that it corresponds to the ternary Cu_2SnS_3 phase. With further annealing treatment, the intensity of the Cu_2SnS_3 increases with temperature. When the temperature is up to 400°C, the Raman spectrum contains three frequencies, at 287 cm^{-1}, 338 cm^{-1}, and 368 cm^{-1}, which confirms the formation of the kesterite CZTS phase.

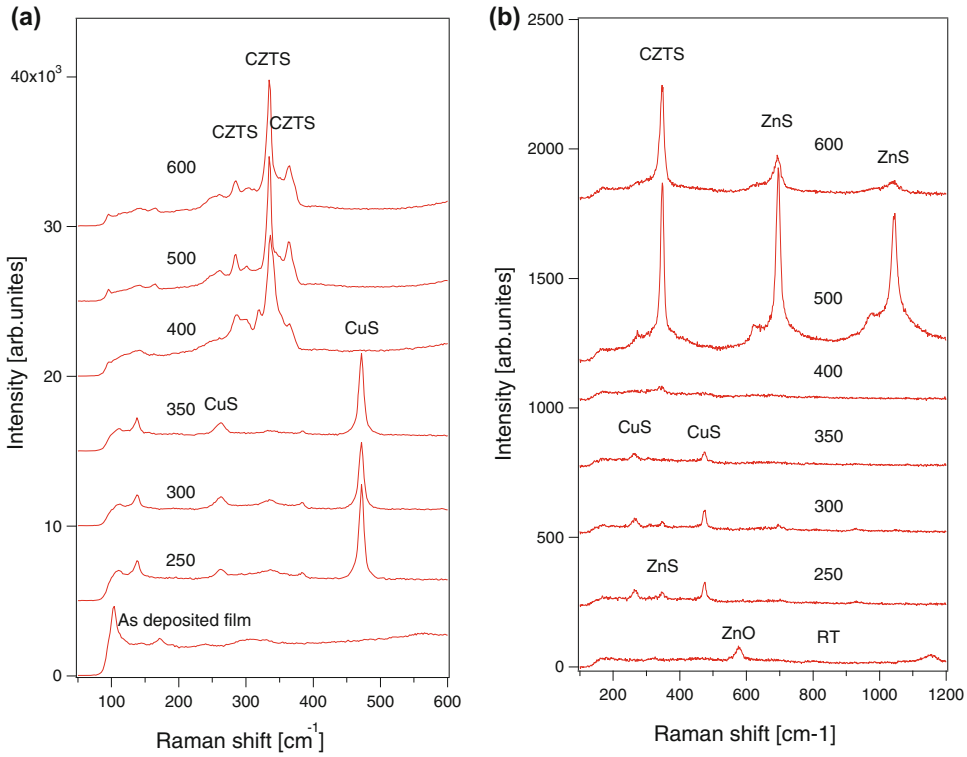

Fig. 2. Raman spectra of the as-deposited film and films annealed at various temperatures from 250°C to 600°C: (a) 633 nm laser; (b) 325 nm laser.

From Fig. 2b (325 nm laser), the formation of a ZnO phase can be observed at the initial precursor which disappears above 250°C. At 400°C, the peak at 1043 cm^{-1}, related to ZnS, shows up on the film surface. The intensity of the ZnS peak increases markedly at 500°C and decreases at 600°C.

XPS Surface Characterization of Thin Films Annealed at Various Temperatures

Figure 3a shows the XPS survey scan spectra made on the CZTS surface. The surface contaminations of C and O are found on all samples (C 1*s* and O 1*s*). The Zn 2*p* and Sn 3*d* are detected in the precursor film. The intensity of these peaks decreases considerably in the temperature range of 250–350°C. Simultaneously, Cu 2*p* and S 2*p* peaks become clear in the spectra. Above 400°C, all elements including Cu, Zn, Sn and S are detected on the film surfaces. To investigate the chemical states of all those elements, the XPS core levels of Cu 2*p*, Zn 2*p*, Sn 3*d*, S 2*p* and Na 1*s* have been deconvoluted and shown in Fig. 3b–f.

Starting from Cu $2p_{3/2}$ core levels, a weak Cu signal is observed in the precursor surface. Above 250°C, the intensity of the Cu signal strongly increases. The curve fitting results indicate that the Cu 2*p* peaks above 250°C are composed of four components (inset in Fig. 3b). The main peak is near 932 eV (250–400°C) and it shifts slightly towards lower binding energy for the samples annealed above 400°C. Considering Raman analysis, we conclude that it may relate to Cu^+ ions, mainly in Cu_2S at 250–400°C and Cu_2ZnSnS_4 above 400°C. The presence of other peaks at a higher binding energy indicates either Cu^{2+} formation or other chemical compounds such as $Cu_{1-x}S$ (933.6 eV), CuS (934.8 eV) and $CuCO_3$ (936.1 eV). The intensity of these peaks decreases above 400°C. The XPS results show that the CZTS films contain complicated chemical states on the surface.

Figure 3c and d show the Zn $2p_{3/2}$ and Sn $3d_{5/2}$ peaks. The peak intensities of these elements are low and increase above 400°C annealing temperature. The curve fitting analyses indicate that the samples have only two chemical states for both kinds of spectra (insets in Fig. 3c and d, respectively). For the Zn 2*p* peaks, the lower part may be related to Zn^{2+} and surrounded with S, while the higher component is related to ZnO. We could also observe the two components from the Sn 3*d* peaks: the higher one may correspond to SnO. Neither Zn and Sn are as sensitive as Cu 2*p* related to their chemical surrounding. S 2*p* peaks are shown in Fig. 3e. The curve fitting analyses indicate that the samples have three chemical states on the surface of samples below 400°C (inset in Fig. 3e). Considering the Raman results, we can assume that the two components with higher binding energies may be related to the binary phases like Cu_2S or CuS. In Fig. 3f, no Na 1*s* signal is found below 300°C, but above 350°C, a slight increase of the Na 1*s* peak is identified.

The Chemical Composition Evolution of CZTS Thin Film Surface Under Various Annealing Temperatures

The chemical composition of thin film surface was characterized by using XPS. Figure 4 shows the evolution of the chemical compositions of thin film surfaces under various temperatures. Due to the sputtering sequence of Cu/Sn/Zn, the initial Cu/(Zn+Sn) and Zn/Sn composition ratio is 0.04 and 2.8 on the film surface, respectively. This indicates the presence of a large quantity of Zn on the film surface. After annealing at 250°C, the ratio of Cu/

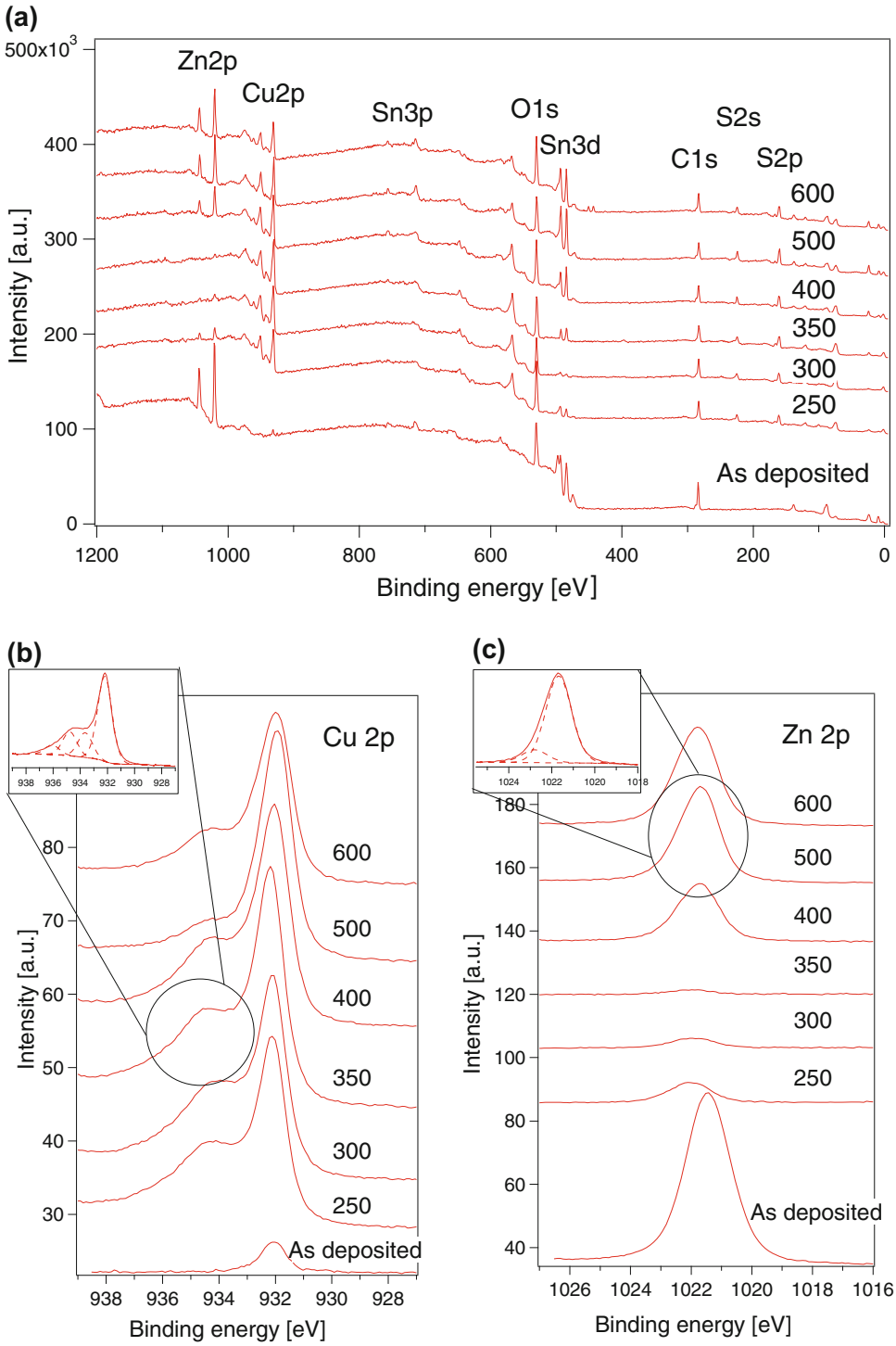

Fig. 3. XPS survey scans and core levels of the as-deposited film and films annealed at various temperatures from 250°C to 600°C: (a) survey scans; (b) Cu 2*p*; (c) Zn 2*p*; (d) Sn 3*d*; (e) S 2*p*; (f) Na 1*s*.

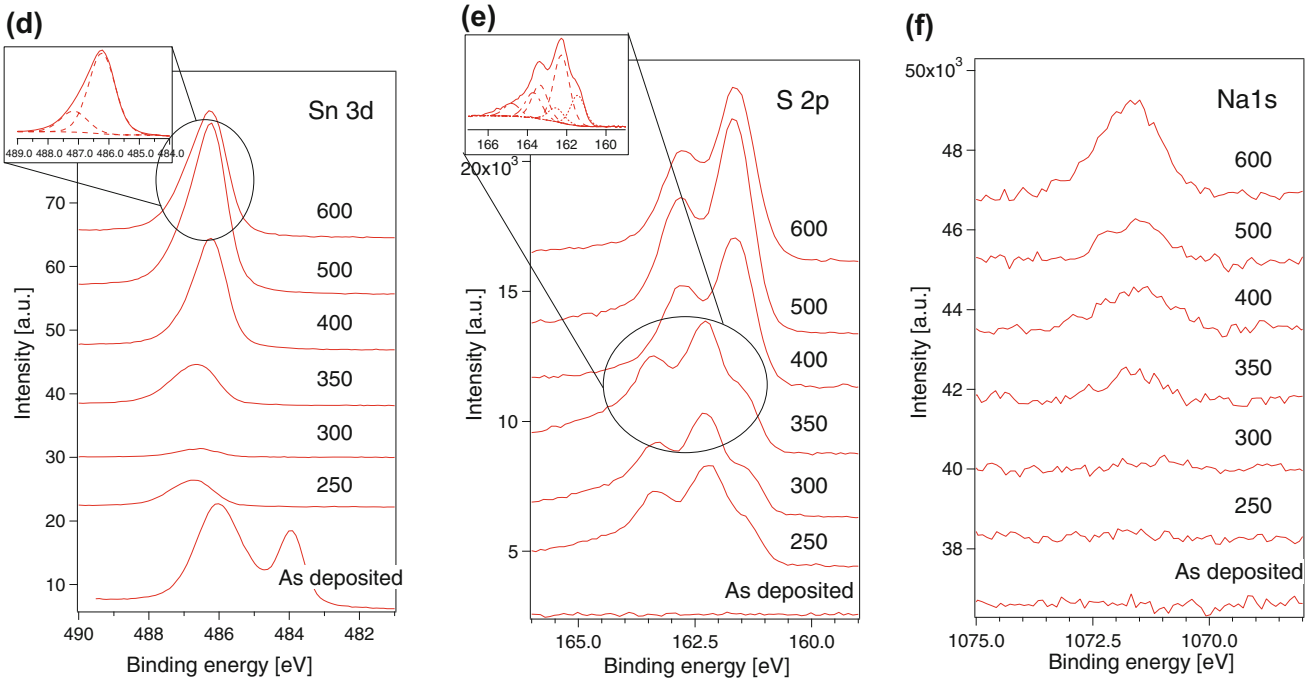

Fig. 3. continued.

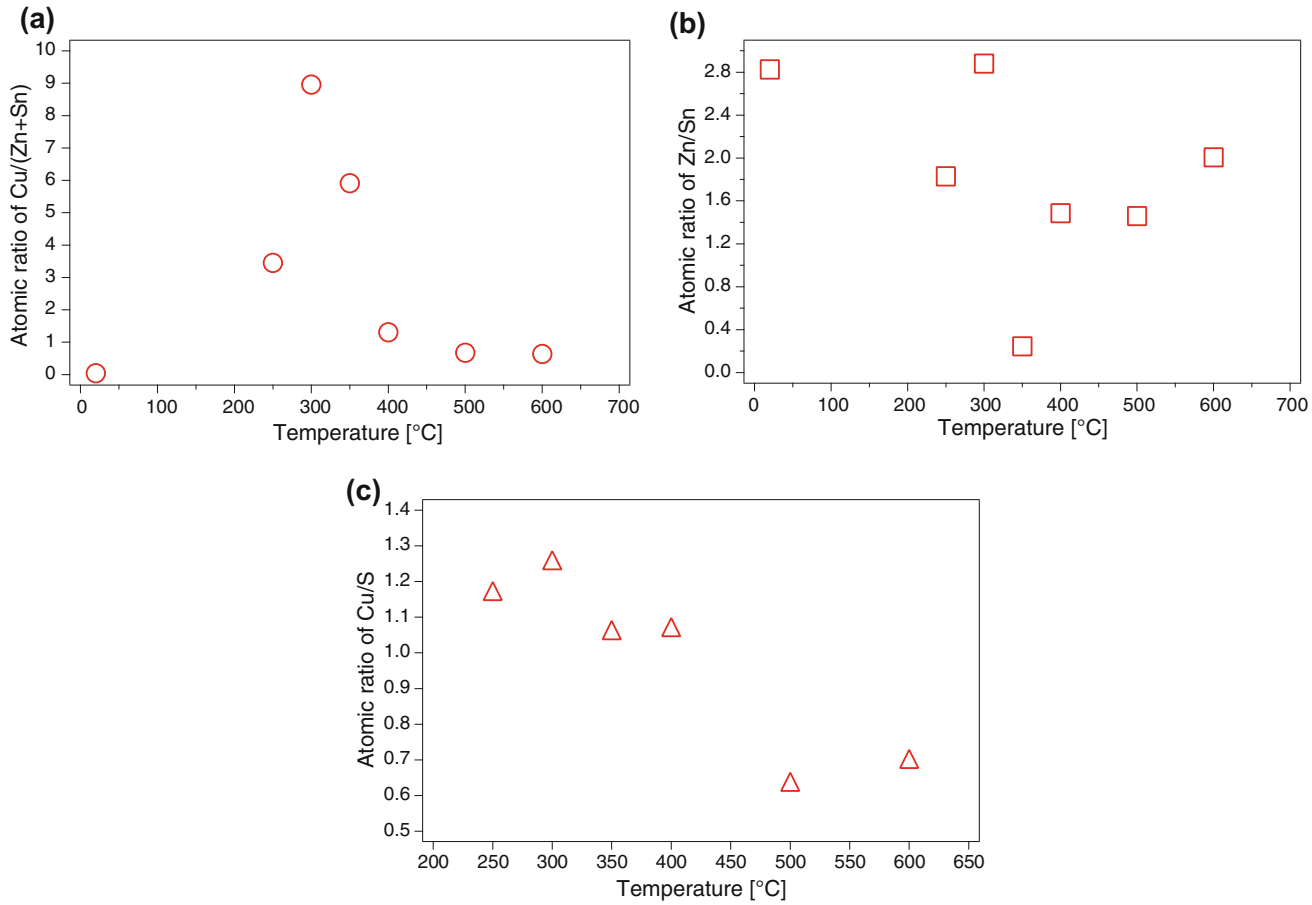

Fig. 4. XPS analyses of the as-deposited film and films annealed at various temperatures from 250°C to 600°C: (a) Cu/(Zn+Sn) ratio; (b) Zn/Sn ratio; (c) Cu/S.

(Zn+Sn) increases to 2.4. Considering the Cu/S ratio 1.17, the Cu-related components such as $Cu_{1-x}S$, are formed on the surface. It is a good agreement with Raman spectra analysis results. At 300°C, the ratio of the Cu/(Zn+Sn) increases further to 8.9, and Cu/S ratio remains at 1.2, which means that the surface is completely covered by $Cu_{1-x}S$. With further increasing in the temperature (350°C), the ratio of Cu/(Zn+Sn) starts to decrease to 5.9, and simultaneously the ratio of Cu/S becomes 1.0. At 400°C, Zn and Sn peaks become stronger. The ratio of Cu/(Zn+Sn) decreases down to 1.3, and the Zn/Sn is 1.5, which is near the bulk composition. Further increasing the anneal temperature causes an obvious decrease of the Cu amount on the surface at 500°C. The Cu/(Zn+Sn) becomes 0.6, indicating a Cu-poor surface. The Zn/Sn ratio decreases slowly to 1.4. Finally, at 600°C, the value of Cu/(Zn+Sn) remains at 0.6 while the Zn/Sn ratio increases to 2.0. As identified in the Raman measurements, a Cu poor and Zn rich surface is formed at this temperature. From the XPS spectra, we also observe Na signals on the surface above 350°C. The Na concentration increases at higher temperatures from 350°C to 600°C, and at 600°C, the Na concentration reaches 5%.

Using the SEM, Raman and XPS analyses together, the CZTS surface evolution during annealing can be seen clearly. The surface of the as-sputtered precursor contains little Cu and large amounts of Zn and Sn. With the increase in temperature, Cu atoms diffuse to the film surface to form $Cu_{1-x}S$ and cover other compounds. When the temperature reaches 350°C, the Zn and Sn atoms begin to diffuse to the surface and react with S or $Cu_{1-x}S$. Because of the Cu-poor and Zn-rich precursor, excess Zn segregates towards the surface regions above 500°C as shown by both Raman spectra and XPS analysis. Simultaneously, the surface becomes Cu-poor, which is similar to the observations in $CuInSe_2$ and $CuInS_2$ research work.[25] Interestingly, sodium is detected on the CZTS surface above 400°C. Although sodium plays an important role in CIGS solar cells, the related research work on Na in CZTS film is still not very clear and further investigation is necessary.

CONCLUSION

In this work, we prepared CZTS films by sputtering precursors and a subsequent annealing process under various temperatures in Ar and H_2S atmosphere. The surface evolution was investigated carefully by using SEM, Raman spectroscopy and XPS. The ZnO phase was detected on the surface of the precursor. Between 250°C and 300°C, the surface showed a porous structure with a lot of pinholes and cracks among the grain boundaries, and was covered by some Cu-Se compounds according to the Raman analyses. Above 400°C, the large particles melted and clear edges disappeared, and the film consisted of small particles with a size from 100 nm to 200 nm and the CZTS phase was formed. Simultaneously, the ZnS phase appeared in the surface with increased temperature. The surface became Cu-poor and Zn-rich. In addition, Na signals were detected in the film surface at high temperatures. At 600°C, a large amount of grains with clear edges and corners were observed in the film surface. Due to the recrystallization process, a denser and compact film was formed. As a result, we could suggest a film recrystallizing process at that temperature.

ACKNOWLEDGEMENTS

The authors acknowledge the financial support of Beijing Institute of Technology Research Fund Program for Young Scholars and National Nature Science Foundation of China (51502015 and 51402103).

REFERENCES

1. T. Nakada, *Electron. Mater. Lett.* 8, 179 (2012).
2. M. Edoff, *AMBIO* 41, 112 (2012).
3. J. Yang, J. Nam, D. Kim, D. Lee, and P. Huh, *Sol. Energy Mater. Sol. Cells* 144, 467 (2016).
4. M.A. Green, K. Emery, Y. Hishikawa, W. Warta, and E.D. Dunlop, *Prog. Photovolt. Res. Appl.* 24, 3 (2016).
5. US Geological Survey, *Mineral Commodity Summaries 2012* (Washington, DC: United States Government Printing Office, 2012).
6. P. Zawadzki, L.L. Baranowski, H. Peng, E.S. Toberer, D.S. Ginley, W. Tumas, A. Zakutayev, and S. Lany, *Appl. Phys. Lett.* 103, 253902 (2013).
7. R.E. Ornelas-Acosta, S. Shaji, D. Avellaneda, G.A. Castillo, T.K. Das Roy, and B. Krishnan, *Mater. Res. Bull.* 61, 215 (2015).
8. H. Song, X. Zhan, D. Li, Y. Zhou, B. Yang, K. Zeng, J. Zhong, X. Miao, and J. Tang, *Sol. Energy Mater. Sol. Cells* 146, 1 (2016).
9. H. Chen, Q. Ye, X. He, J. Ding, Y. Zhang, J. Han, J. Liu, C. Liao, J. Mei, and W. Lau, *Green Chem.* 16, 3841 (2014).
10. S. Siebentritt and S. Schorr, *Prog. Photovolt. Res. Appl.* 20, 512 (2012).
11. M.P. Suryawanshi, S.W. Shin, U.V. Ghorpade, C.W. Hong, P.S. Patil, A.V. Moholkar, and J.H. Kim, *J. Alloys Compd.* 671, 509 (2016).
12. M. Abusnina, H. Moutinho, M. Al-Jassim, C. DeHart, and M. Matin, *J. Electron. Mater.* 43, 3145 (2014).
13. H. Guan, H. Shen, C. Gao, and X. He, *J. Mater. Sci. Mater. Electron.* 24, 2667 (2013).
14. Y. Zhang, C. Liao, K. Zong, H. Wang, J. Liu, T. Jiang, J. Han, G. Liu, L. Cui, Q. Ye, H. Yan, and W. Lau, *Sol. Energy* 94, 1 (2013).
15. W. Wang, M.T. Winkler, O. Gunawan, T. Gokmen, T.K. Todorov, Y. Zhu, and D.B. Mitzi, *Adv. Energy Mater.* 4, 1301465 (2014).
16. S. Siebentritt, *Thin Solid Films* 535, 1 (2013).
17. M. Kumar, A. Dubey, N. Adhikari, S. Venkatesan, and Q. Qiao, *Energy Environ. Sci.* 8, 3134 (2015).
18. W. Hsu, I. Repins, C. Beall, C. DeHart, G. Teeter, B. To, Y. Yang, and R. Noufi, *Sol. Energy Mater. Sol. Cells* 113, 160 (2013).
19. J. Li, H. Wang, M. Luo, J. Tang, C. Chen, W. Liu, F. Liu, Y. Sun, J. Han, and Y. Zhang, *Sol. Energy Mater. Sol. Cells* 149, 242 (2016).
20. H.R. Jung, S.W. Shin, K.V. Gurav, M.G. Gang, J.Y. Lee, J.H. Moon, and J.H. Kim, *Electron. Mater. Lett.* 12, 139 (2016).

21. D.M. Berg, M. Arasimowicz, R. Djemour, L. Gütay, S. Siebentritt, S. Schorr, and X. Fontané, *Thin Solid Films* 569, 113 (2014).
22. S. Chen, A. Walsh, X. Gong, and S.-H. Wei, *Adv. Mater.* 25, 1522 (2013).
23. P.K. Sarswat and M.L. Free, *J. Mater. Sci.* 50, 1613 (2015).
24. H.R. Jung, S.W. Shin, K.V. Gurav, M.P. Suryawanshi, C.W. Hong, H.S. Yang, and J.Y. Lee, *Ceram. Int.* 41, 13006 (2015).
25. J. Han, L. Ouyang, D.-M. Zhuang, M. Zhao, C. Liao, J. Liu, L. Cha, and M.-P. Besland, *J. Mater. Sci. Mater. Electron.* 26, 4840 (2015).